American Mineralogist, Volume 88, pages 1769–1777, 2003

# The aperiodic states of zircon: an ab initio molecular dynamics study

ETIENNE BALAN,[1,2,*] FRANCESCO MAURI,[1] CHRIS J. PICKARD,[3] IAN FARNAN,[4] AND GEORGES CALAS[1]

[1]Laboratoire de Minéralogie-Cristallographie, UMR CNRS 7590, Universités Paris 6 et 7, IPGP, 4 Place Jussieu, 75252 Paris Cedex 05, France
[2]Institut de Recherche pour le Développement (IRD), UR 058, 213 rue LaFayette, 75480 Paris cedex 10, France
[3]TCM Group, Cavendish Laboratory, University of Cambridge, Madingley Road, Cambridge, CB3 OHE, U.K.
[4]Department of Earth Sciences, University of Cambridge, Downing Street, Cambridge, CB2 3EQ, U.K.

## ABSTRACT

We theoretically investigated the local structure of the aperiodic states of zircon ($ZrSiO_4$) using ab initio quantum mechanical calculations. The low and high density liquid and solid glassy phases were obtained by constant volume Car-Parrinello molecular dynamics simulations, using the molar volume of metamict and crystalline zircon, respectively. As in naturally metamict zircons, the polymerization of Si units, the segregation of Zr atoms, and an overall decrease of the Zr coordination were observed. However, the local ordering of our theoretical glasses differs from that of the natural amorphous samples. In the theoretical glasses, the Zr-O distances in the first coordination polyhedra are significantly more distributed and five- and six-coordinated Si species were observed. The relaxation of the glass structure on a time scale exceeding the possibility of molecular modeling is a possible explanation for these discrepancies. The dielectric and $^{29}$Si NMR responses of the glassy phases were computed, providing new constraints for the analysis of experimental data recorded from metamict zircons. The calculated NMR spectra are in good agreement with the experimental NMR spectra in the four-coordinated Si region. Our results show that the usual regular systematic decrease of the $^{29}$Si chemical shift as a function of the polymerization of Si units ($Q^n$ species) cannot be used to interpret the $^{29}$Si NMR spectrum of amorphous zircon. In particular, whereas the empirical scale would indicate an average polymerization of $Q^3$, the average polymerization of $Q^{1.5}$ observed in the low density zircon glass can account for the experimental data. In a non-uniform model of the structure of metamict zircon, this lower average polymerization is consistent with a clustering of cations limited to few coordination polyhedra.

## INTRODUCTION

The amorphization of zircon has been the focus of considerable attention because of its geochemical and technological implications. It occurs naturally as a result of the accumulation of radiation damage over time (Holland and Gottfried 1955). In this case, the amorphization was related to the radioactive decay of U and Th incorporated during growth of the crystal. This process dramatically changes the physical and chemical properties of zircon and many studies report the increased reactivity of damaged zircon (Ewing et al. 1982; Ellsworth et al. 1994; Ewing 1999; Balan et al. 2001a; Geisler et al. 2002). The structure of the resulting amorphous phase likely determines the dissolution and recrystallization mechanisms of damaged zircon and controls the bulk diffusion of trace elements in metamict zircons. Since zircon has been proposed for the encapsulation of high-level radioactive wastes, its radiation-induced amorphization has been widely studied, both in natural samples and in samples implanted with heavy ions. A remarkable similarity has been found between naturally and experimentally amorphized zircons. Amorphous $ZrSi_xO_y$ samples have also been synthesized in thin films by comagnetron-reactive sputtering (Qi et al. 2000). These high permittivity films were actively investigated because they could replace conventional oxide or oxynitride films in new metal-oxide-semiconductor (MOS) devices (Wilk et al. 2000; Rignanese et al. 2002).

In the natural amorphization process induced by radiation damage, α-recoil nuclei directly amorphize nanometric volumes of the structure, whereas an increase of the unit-cell volume was observed in the nearby still-periodic structure (Salje et al. 1999; Ríos et al. 2000). This results in the coexistence, at a sub-micrometric scale, of crystalline and amorphous domains, which can be observed by transmission electron microscopy (Murakami et al. 1991; Weber et al. 1994). Because of the random accumulation and overlap of the amorphous domains, zircon progressively reaches a macroscopic quasi-amorphous state, referred to as the metamict state (Salje et al. 1999). The structural changes associated with amorphization include a decrease in the Zr coordination, observed by extended X-ray absorption fine structure spectroscopy (EXAFS) at the Zr *K*-edge of metamict zircons (Farges and Calas 1991), and the polymerization of Si species, which causes a strong shift and broadening of the $^{29}$Si NMR signal (Farnan and Salje 2001). In addition, changes in the structure of the amorphous phases between weakly and highly damaged samples were suggested by X-ray scattering (Ríos et al. 2000) and nuclear magnetic resonance investigations (Farnan 1999; Farnan and Salje 2001). These changes were correlated with the significant macroscopic swelling observed in metamict zircon, which reaches 18% in the more damaged samples.

* E-mail: Etienne.Balan@lmcp.jussieu.fr

The formation of nanometric amorphous domains in natural zircon is the result of ballistic collisions triggered by α-recoil nuclei. Classical molecular dynamics modeling of radiation damage in zircon have shown the formation of polymerized $SiO_4$ units in the amorphous phase together with a decrease in the Zr coordination number and the occurrence of five and sixfold coordinated Si species (Trachenko et al. 2001; Crocombette and Ghaleb 2001). However, no experimental evidence of the occurrence of highly coordinated Si species was found in the NMR spectra of metamict zircon (Farnan and Salje 2001). A recent molecular dynamics study of high energy α-recoil in zircon has also suggested that the damaged region is highly heterogeneous, exhibiting a low density core surrounded by a sphere of polymerized and densified material (Trachenko et al. 2002). According to this last study, the overlap between the damaged regions is expected to produce the macroscopic swelling of metamict zircon.

The temperature dependence of the radiation dose needed to amorphize the structure has suggested the existence of a transient liquid-like state in the displacement cascades (Meldrum et al. 1998; Wang et al. 2000). Consistently, molecular dynamics indicates that the temperature in the cascade of defects could exceed the melting temperature of zircon for a short time (Crocombette and Ghaleb 2001). Thus, despite different production mechanisms, the local structure of amorphous domains in metamict zircon could share some similarities with that of a rapidly quenched glass of zircon composition. Unfortunately, such a glass cannot be experimentally obtained because of the rapid unmixing of Zr oxide in the high temperature liquid.

In the present study, we theoretically investigated the local structure of this system, i.e., the liquid and solid amorphous states of zircon, using constant volume ab initio molecular dynamics. However, the computational expense of first-principle calculations imposes limitations on the size of the investigated system. For this reason we mainly focused on the first and second neighbors coordination shell of the cations. Given the significant macroscopic swelling observed in natural zircon as a function of the degree of metamictization, we considered two different molar volumes. The high density (HD) liquid and solid phases were obtained using the experimental molar volume of crystalline zircon (Hazen and Finger 1979), whereas the low density (LD) phases were obtained after a relative swelling of 18%, which corresponds to that observed in the natural samples of amorphous zircon. Accordingly, the structural and spectroscopic properties of the HD and LD solid glassy phases were compared to the experimental results obtained from weakly (dose $< 3 \times 10^{15}$ α-decay/mg) and highly (dose $> 8 \times 10^{15}$ α-decay/mg) damaged zircon samples, respectively. In particular, we computed the $^{29}$Si NMR responses of the two solid states, introducing new constraints for the analysis of experimental data.

## Computational methods

Accurate modeling of the crystal structure of zircon has been previously achieved within the framework of density functional theory (Crocombette and Ghaleb 1998; Balan et al. 2001b; Rignanese et al. 2001; Farnan et al. 2003). In the present study, ab initio molecular dynamics was performed using the Car-Parrinello molecular dynamics scheme (Car and Parrinello 1985). We used the generalized gradient approximation to the density functional as proposed by Perdew, Burke, and Ernzerhof (PBE) (Perdew et al. 1996). The ionic cores were described by norm-conserving pseudo-potentials (Troullier and Martins 1991) in the Kleinman-Bylander form (Kleinman and Bylander 1982). The wave-functions and the charge density were expanded in plane-waves with 50 and 200 Ry cutoffs, respectively (Balan et al. 2001b). The Hamiltonian cutoff for the mass preconditioning and the fictitious electron mass in molecular dynamics were set at 4 Ry and 200 a.u., respectively, and a timestep of 4 a.u. was used. The ionic temperature was controlled using a Nosé-Hoover thermostat of frequency 500 $cm^{-1}$. The electronic temperature was not thermostated. The Brillouin zone was sampled at the Γ point and the calculations were performed with the CPMD program (Hutter et al. 1996). Structure relaxations with the CPMD code were performed until the forces on the atoms were smaller than $5 \times 10^{-2}$ eV/Å using a cutoff of 50 Ry for the wave-functions. The pressure was calculated on selected configurations of the system as a third of the trace of the stress tensor. For this calculation, the cutoff for the wave-functions and the charge density was increased to 100 and 400 Ry, respectively, because of the slow convergence of the stress tensor with respect to the size of the plane-waves basis set. When increasing the cutoff for the wave functions to 100 Ry, the forces on the atoms of the relaxed structures remained smaller than $1.5 \times 10^{-1}$ eV/Å.

The NMR $^{29}$Si chemical shifts were obtained by calculating the shielding of the $^{29}$Si nuclei due to the electronic current induced by an external magnetic field. This current was calculated using the GIPAW approach, which allows the reconstruction of the all-electron electronic structure from pseudo-wave-functions (Pickard and Mauri 2001). Relative values of the chemical shifts can therefore be obtained from our pseudo-potential approach with the accuracy of a fully converged all-electron calculation. The chemical shift scale was fixed in such a way that the $^{29}$Si chemical shift computed for crystalline zircon coincided with the experimental value (–81.5 ppm). The calculations were performed using the PARATEC code (Pfrommer et al., http://www.nersc.gov/projects/paratec) with a cutoff of 70 Ry for the wave-functions. The accuracy of this approach was determined by computing the $^{29}$Si chemical shift in reidite, the high pressure phase of zircon. The difference observed between theory and experiment was smaller than 1 ppm (Farnan et al. 2003).

The low-frequency dielectric tensors of the LD glass and of the crystalline zircon were calculated following the approach detailed in Balan et al. (2001c). The dynamical matrix was obtained with a cutoff of 50 Ry for the wave-functions using the finite difference approach implemented in the CPMD code. The effective charges and the electronic contribution to the dielectric tensor were derived using the density functional perturbation theory (Baroni et al. 2001). For this last calculation, the PWSCF and PHONON codes were used (S. Baroni, A. Dal Corso, S. de Gironcoli, and P. Giannozzi. http://www.pwscf.org/) with a cutoff of 50 Ry for the wave-functions.

Because of differences in the implementation of the plane-wave codes and in the generation of the pseudopotentials, some of the forces computed with the PWSCF and PARATEC codes for the CPMD-optimized structures consistently increased to $5 \times 10^{-1}$ eV/Å. These small forces do not affect the spectroscopic properties of the structures relaxed with CPMD, which were thus calculated without further relaxation.

## Results

### Generation of the amorphous phases

The liquid and glassy states of zircon were obtained using constant volume ab initio molecular dynamics. We used periodically repeated supercells containing 16 $ZrSiO_4$ units, i.e., 96 atoms. Experimentally determined cell parameters of zircon ($a = 6.6042$ Å, $c = 5.9796$ Å; Hazen and Finger 1979) were used to define the supercell of the HD system. Since the statistical expectation value of an observable that depends just on the position (e.g., the structure) does not depend on the ionic masses in classical mechanics (Frenkel and Smit 1996), the Si and Zr masses were scaled to the O mass to increase the diffusion rates of the cations. The starting crystal structure was heated to 5000 K over 1 ps (Fig. 1). The system was allowed to evolve at 5000 K for 2 ps and then was quenched to 0 K in 1 ps, leading to the high density glassy state (HD glass; Fig. 2). The diffusion of Zr and Si cations in the high temperature liquid

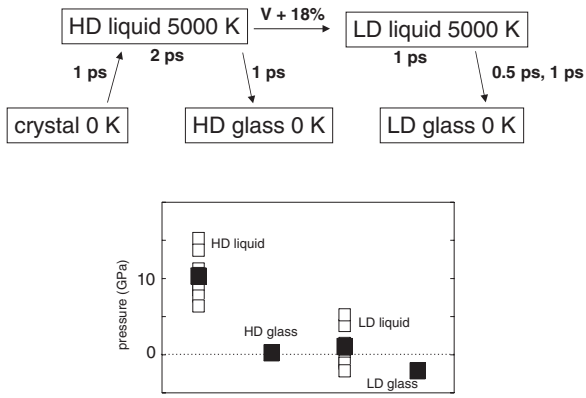


**FIGURE 1.** Scheme of the molecular dynamics simulations. In the bottom panel, the pressure of the solid state and that of selected liquid configurations is reported (white squares). The black squares represent average value of pressure in liquid and solid states.

state is attested by their final mean square displacements of ~12 Å$^2$. However, because of the mass change of the cations, diffusion coefficents could not be determined from the present study. The pressure over the liquid state ranged from 5 to 15 GPa, whereas the corresponding high density glassy state was at a pressure close to zero (0.3 GPa). In a second step, the molar volume of the liquid at 5000 K was increased by 18%, which is the swelling experimentally observed in metamict zircons, and the corresponding low density liquid state was equilibrated for 1 ps. The pressure over the LD liquid state ranged between –5 and 5 GPa. Two quenches of the LD liquid state were performed in 0.5 and 1 ps, respectively (Fig. 1). The corresponding quenching rates, $10 \times 10^{15}$ and $5 \times 10^{15}$ K/s, respectively, were very high. They were larger by several orders of magnitude than those which can be achieved experimentally by the quenching of liquid silicate melts. However, our quenching rates were comparable to those observed in the simulation of cascades in zircon (Crocombette and Ghaleb 2001; Trachenko et

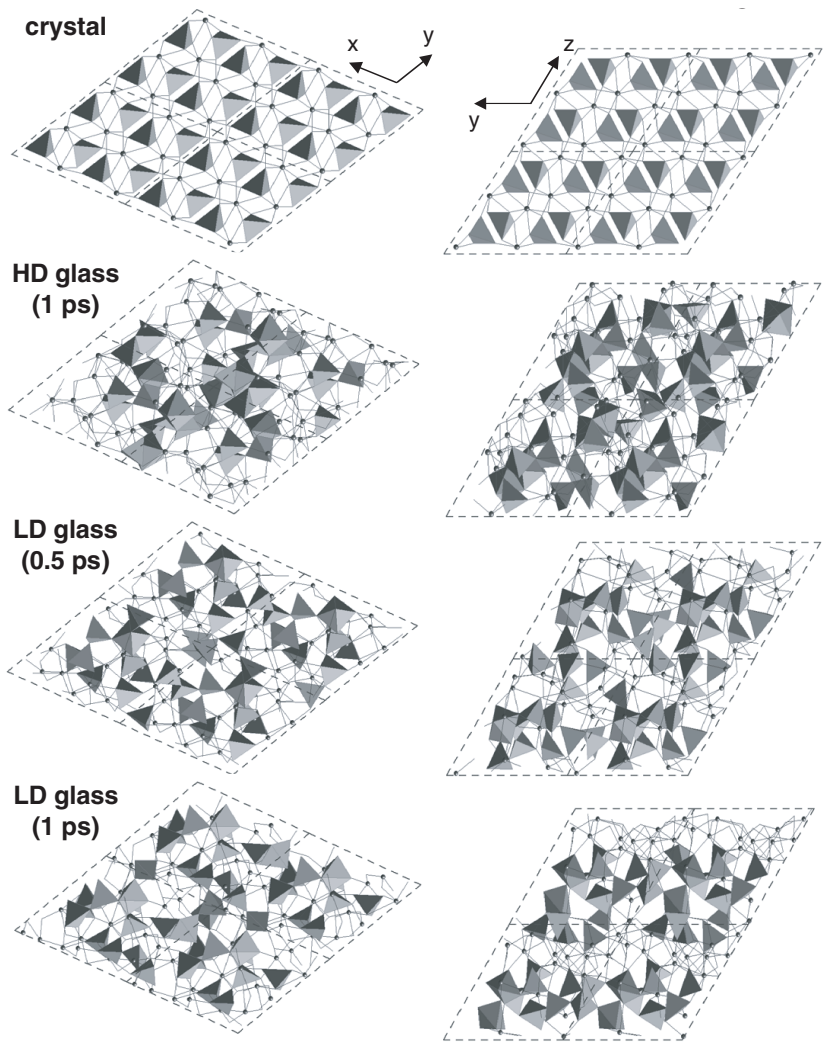


**FIGURE 2.** Structure of the crystalline and glassy states of zircon. In each plot, four unit cells (each containing 96 atoms) used in the periodic modeling are represented. Note the occurrence of highly coordinated Si species, the polymerization of Si units, and the clustering of Zr atoms in the glassy phases. Polyhedra = Si units, sphere = Zr atoms.

**TABLE 1.** Structural characterictics of the HD and LD zircon glasses

| | $^{IV}$Si | $^{V}$Si | $^{VI}$Si | $Q^0$ | $Q^1$ | $Q^2$ | $Q^3$ | Other* | Si-O-Si | Zr-O-Zr |
|---|---|---|---|---|---|---|---|---|---|---|
| HD | 10 | 2 | 4 | 1 | 1 | 0 | 0 | 8 | 13 | 12 |
| LD1 | 15 | 0 | 1 | 1 | 5 | 6 | 0 | 3 | 17 | 16 |
| LD2 | 14 | 1 | 1 | 2 | 4 | 1 | 1 | 6 | 15 | 16 |

*Notes:* LD1 and LD2 correspond to quench times of 0.5 and 1 ps, respectively. *other: $^{IV}$Si connected with $^{V}$Si or $^{VI}$Si.

al. 2002; Devanathan et al. 2002). Despite a more apparent clustering of Zr atoms following the 1 ps quench (Fig. 2), the polymerization of the Si species (Table 1) and the radial interatomic distances distribution functions were very similar. Given the small size of the system, the small differences observed, e.g., the occurrence of an additional fivefold coordinated Si in the second quench (Table 1), were most likely related to statistical fluctuations of the glass structure. The statistical analysis of the LD glass was thus performed by averaging the two LD structures. The pressure over the LD glass state was slightly negative (–2 GPa). Note that using density functional theory and starting from the crystal structure, we observed a diffusive behavior at 5000 K, whereas classical molecular dynamics require a significantly higher temperature (10 000 K) to observe diffusion (Crocombette and Ghaleb 2001; Devanathan et al. 2002).

### Structure of the aperiodic states of zircon

The average Si-O pair correlation functions of the liquid and glassy states of zircon show a well defined first peak at 1.68 Å (Fig. 3). Except for a large temperature broadening, the Si-O pair correlation functions are similar for the liquid and the glassy states. The peak observed at 1.68 Å corresponds to a significant increase in the Si-O distance compared to that in the crystal structure (1.62 Å).

The coordination of Si atoms can be investigated as a function of the coordination sphere radius (Fig. 4). The resulting distribution of Si species shows significant changes among the various aperiodic states of zircon. In both liquid states, the fourfold coordination corresponds to only about sixty percent of the silicon atoms. In the HD liquid state, other Si species are distributed between threefold coordinated Si atoms and highly coordinated species (five and sixfold coordinated Si atoms). In contrast, the LD liquid state shows an overall decrease in the number of highly coordinated Si atoms, which were observed at higher cutoff radii. Such changes are consistent with a decrease in the pressure of the liquid. Compared with the liquid states, the solid glassy states were characterized by a strong recovery of fourfold coordination and the disappearance of threefold coordinated species. Using a radius of 2.3 Å for the first coordination shell of Si, the HD glass phase still contains a significant amount of five and sixfold coordinated Si atoms, whereas the LD glass contains mainly tetrahedral Si species (Table 1). To assess the stability of the highly coordinated Si species observed in the HD glass with respect to a simple volume change, the molar volume of the HD glass was increased to the LD molar volume. The forces appearing on the atoms were then minimized by performing a molecular dynamics simulation during which the atomic velocities were progressively decreased (relaxation by simulated annealing). During this simulation, the temperature continuously decreased from 3700 to 500 K in ~0.03 ps and the mean square displacement of the cations was limited to ~0.2 Å$^2$, which means that no significant diffusion occurred. The resulting LD glassy state was thus produced by a solid state transformation of the HD glass. This transformation only decreased the coordination of the sixfold coordinated Si atoms to a fivefold coordination, whereas the abundance of tetrahedral Si species did not increase. The recovery of the fourfold coordination observed in the LD glass was thus specifically due to the structural changes related to the density changes occurring in the liquid state.

The average Zr-O pair correlation functions of the liquid

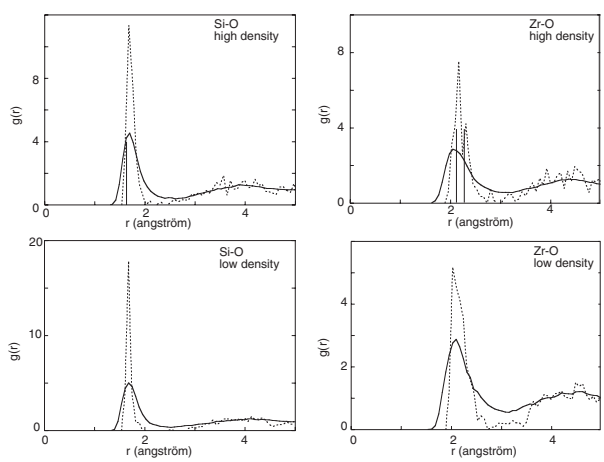


**FIGURE 3.** Cation-O atom pair correlation functions. Continuous line = liquid state, dotted line = solid state. The vertical bars in the plots of the high-density phases represent the cation-O atom distances in the crystal.

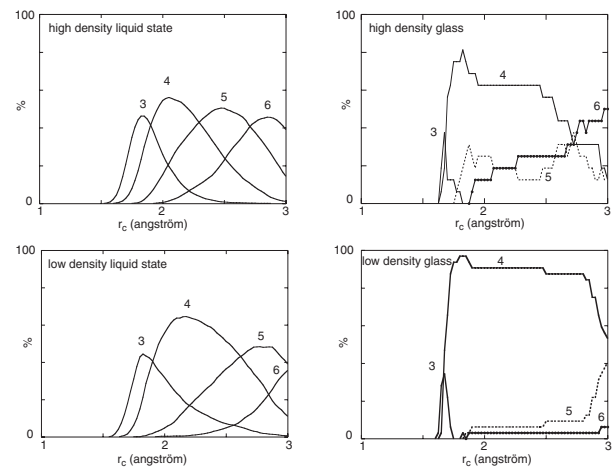


**FIGURE 4.** Si coordination as a function of the coordination sphere radius. Note the persistence of five and sixfold coordinated species in the glasses.

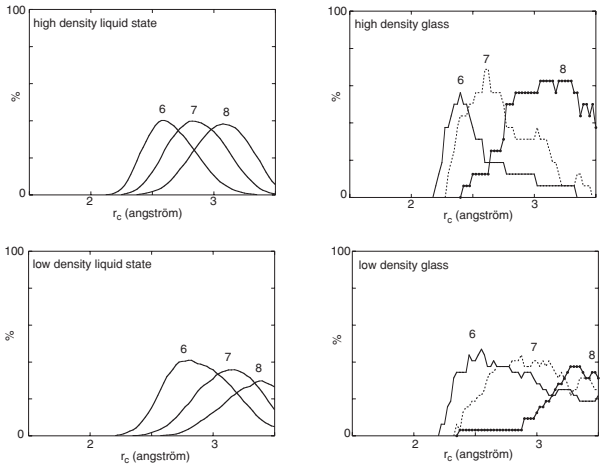


**FIGURE 5.** Zr coordination as a function of the coordination sphere radius. Note the overall decrease in Zr coordination compared to the eightfold coordination in the crystal.

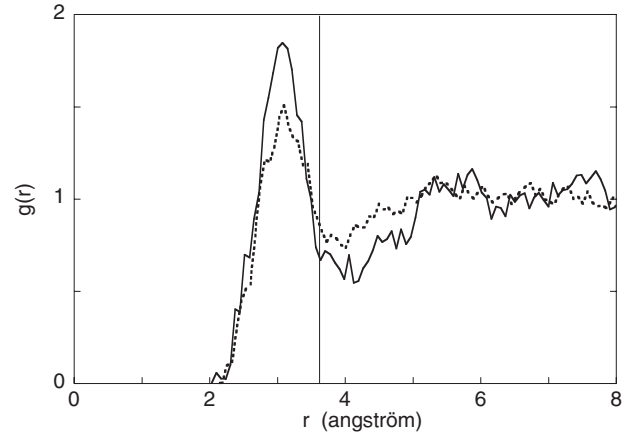


**FIGURE 6.** Si-Si pair correlation functions of the liquid states. The vertical line represents the Si-Si distance in the crystal. The peak observed at 3 Å indicates the polymerization of Si units in the liquid states. Dotted line = high density liquid, continuous line = low density liquid.

and solid glassy states of zircon show a first peak at 2.07 Å (Fig. 3), indicating a shortening of the Zr-O bond in the aperiodic states with respect to the crystalline zircon (2.13 and 2.27 Å). This shortening is consistent with a decrease in the average coordination around the Zr atoms, which is eightfold in the crystal structure. As shown by the distribution of Zr species as a function of the coordination radius (Fig. 5), and considering that the radius of the first coordination sphere is defined by the first minimum of the Zr-O pair correlation function (3 Å), the Zr atoms occur mainly in seven and eightfold and six and sevenfold coordinations in the HD and LD liquid states, respectively. In the solid glassy states, we observed a partial recovery of eightfold coordination for the HD glass, whereas Zr mainly remained in six and sevenfold coordination in the LD glass. Note that this definition of the coordination sphere only relies on geometrical parameters and does not imply a strong chemical bonding between Zr and O atoms. Bond strength calculations for the Zr-O bond, using the bond valence model (Brese and O'Keefe 1991), showed indeed that O atoms farther than 2.5 Å have only a weak bonding interaction with Zr (<0.2 valence unit).

The structural parameters extracted from EXAFS measurements performed at the Zr *K*-edge in naturally metamict zircons indicate that the Zr atoms are surrounded by ~7 O atoms at a distance of 2.13 Å (Farges and Calas 1991). In this case, the mean Zr-O distance of 2.13 Å is similar to that obtained from the crystalline zirconium oxide baddeleyite (2.17 Å), in which the Zr atom is sevenfold coordinated. Our results are consistent with an overall decrease of the Zr coordination. To quantitatively compare theory and experiment, we calculated the theoretical EXAFS spectrum corresponding to the LD glass using the Feff8 code (Ankudinov et al. 1998). After data reduction using a single O shell in the harmonic approximation model, the first coordination shell around Zr was observed in the theoretical LD glass at a distance of 2.02 Å and included ~3 O atoms. The corresponding Debye-Waller term was $\sigma =$ 0.12 Å. The Zr-O distance determined by EXAFS calculation in the theoretical LD glass thus corresponds to the small distance side of the first peak in the theoretical Zr-O pair correlation function. The number of O atoms in the first coordination shell determined by EXAFS calculation is also significantly smaller than the average coordination determined from the Zr-O pair correlation function, which is between six and seven. The EXAFS calculation of a relatively short Zr-O distance and of few nearest neighbors is due to the significant distribution of Zr-O distances in the theoretical LD glass. Indeed, in the case of a continuous distribution of interatomic distances, EXAFS spectroscopy tends to overestimate the short distances and to underestimate the number of atoms in the first coordination shell (Calas and Petiau 1993). The Zr environment is thus significantly more distorted in the LD glass than in the natural samples.

The short Zr-O distances determined experimentally and numerically indicated a coordination change of Zr during metamictization. The Zr-bearing silicate glasses exhibit similar Zr-O distances (2.08 Å). In these glasses, a nonbridging O atom is only bound to one octahedral Zr site, with a charge compensation ensured by alkalis and alkaline earths (Galoisy et al. 1999). In the zircon glasses, such a charge compensation mechanism is not available. Charge compensation necessities on nonbridging O atoms lead to the broad distribution of Zr-O distances and to the lengthening of the Si-O bonds observed in the LD glass.

The analysis of cation-cation pair correlation functions may provide further information on the medium-range structure of the aperiodic systems. In the case of zircon, the observation of a first peak at 3.1 Å in the Si-Si pair correlation functions of the two liquid states (Fig. 6) indicates an onset of polymerization of the Si units, which is more important in the LD liquid. The polymerization is preserved in the solid glassy states and is indicated by the distribution of O atom species. In the LD glass, about 25% of the O atoms bridge two Si atoms and the same proportion is connected to only two or to three Zr atoms (Table 1). Since the stoichiometry of the system is unchanged,

the polymerization of Si units and the clustering of the Zr atoms in Zr-rich domains are correlated, as observed in Figure 2. However, the periodic boundary conditions, together with the relatively small cell size used in the ab initio molecular dynamics calculations, are serious limitations for the discussion of medium-range order in the amorphous states of zircon. In particular, the small changes observed in the Zr-Si and Zr-Zr pair correlation functions cannot lead to an unambiguous interpretation because connections between these cations already exist in the crystal structure of zircon.

### Spectroscopic properties

**Dielectric properties.** The dielectric properties of crystalline zircon have been previously investigated using density functional theory and excellent agreement was found between theory and experiment (rms relative deviations of 2.5% in the phonon frequencies; Rignanese et al. 2001). In our work, the same level of accuracy could not be obtained because of the larger unit cell used to model the amorphous structures. However, the agreement between experiment and calculation is still very good and the differences between the theoretical and experimental frequencies in crystalline zircon do not exceed 30 $cm^{-1}$. A good agreement is also observed with the effective charge tensors and the high-frequency electronic dielectric tensor calculated by Rignanese et al. (2001).

Given the computation time required, the vibrational and dielectric properties of amorphous zircon were only computed for the LD glass quenched in 0.5 ps. The theoretical static $\varepsilon(0)$ and electronic $\varepsilon(\infty)$ dielectric constants of the LD zircon glass are 14.75 and 3.75, respectively. These values correspond to an increase and decrease in $\varepsilon(0)$ and $\varepsilon(\infty)$, respectively, with respect to crystalline zircon (13.0 and 4.24, respectively). The 0.5 unit decrease of $\varepsilon(\infty)$ is in good agreement with that observed between crystalline and metamict zircon (Holland and Gottfried 1955). Following the analysis of Rignanese et al. (2002), this variation is consistent with the decrease of the Zr coordination observed in the LD zircon glass.

The imaginary part of the dielectric constant of the LD zircon glass (Fig. 7) can be directly compared with experimental measurements of metamict zircon (Zhang and Salje 2001). Its theoretical wavenumber dependence shows two main features in the 150–600 and 600–1200 $cm^{-1}$ ranges, respectively. These ranges are in good agreement with the main features experimentally observed. The contribution of the displacement of Zr and Si cations to the imaginary dielectric constant was assessed by computing theoretical partial functions, in which the contribution of a given cation was canceled (Balan et al. 2001c). The Zr contribution was found to extend up to 800 $cm^{-1}$, whereas two major Si contributions were found around 500 and 950 $cm^{-1}$ (Fig. 7). This suggests that the appearance of the extra absorption signal between 400 and 650 $cm^{-1}$ in the experimental spectrum could be related not only to the formation of new Si-O-Si linkages (Zhang and Salje 2001) but also to the distortion of the Zr coordination polyhedra that produces short Zr-O distances. However, the theoretical imaginary dielectric constant exhibits broader features than the experimental one that falls to zero below 200 $cm^{-1}$ and near 800 $cm^{-1}$. This discrepancy is not related only to the presence of crystalline zircon

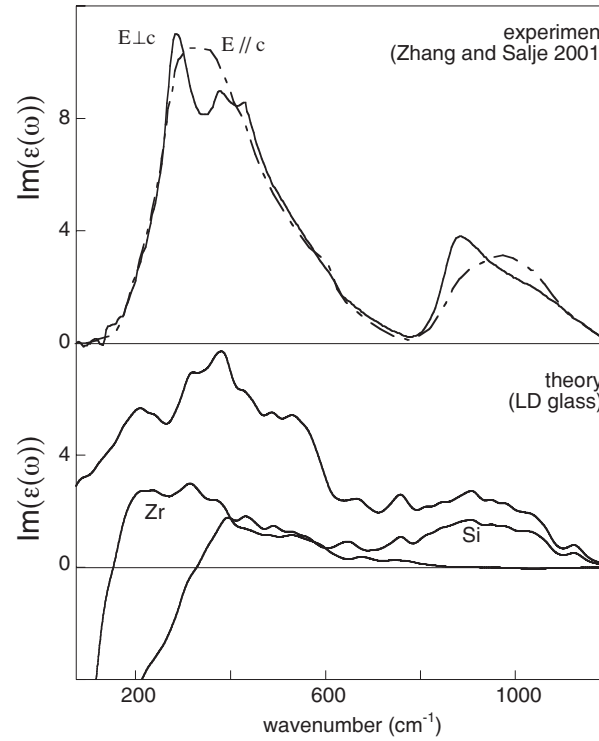


**FIGURE 7.** Theoretical and experimental imaginary dielectric functions. The theoretical function was calculated for the LD glass quenched in 0.5 ps. Experimental functions recorded for two polarizations are related to a highly metamict zircon (Zhang and Salje 2001).

bands in the most damaged samples, which indicates that some local crystalline order still persists in metamict zircon (Zhang and Salje 2001). It also suggests that the LD glass exhibits a greater structural disorder than the amorphous phase occurring in naturally metamict zircon, which is consistent with the information provided by the EXAFS calculations.

**$^{29}$Si NMR spectra.** The NMR $^{29}$Si chemical shifts were calculated for the HD and LD solid glassy states of zircon. To compare these theoretical results with the experimental spectra (Fig. 8), each chemical shift value was convoluted by a Gaussian function with a constant half width of five ppm. Tetrahedral Si species exhibit chemical shifts between –75 and –120 ppm, in good agreement with the width of the broad experimental NMR signal ascribed to the amorphous phase (sample Ham3) and higher signal to noise spectra obtained for zircon UG9A (Farnan and Salje 2001). Interpretation of the NMR spectra of fourfold coordinated Si species is generally performed by considering the linkage of $SiO_4$ units. A regular variation of the chemical shift toward lower values is generally expected when the number of Si second neighbors increases. Compared with the extensively investigated alkali silicate glasses (Maekawa et al. 1991; Stebbins 1995), the chemical shifts observed experimentally for amorphous zircons would predominantly correspond to $Q^2$ or $Q^3$ species, depending on the degree of amorphization of the sample. However, as previously observed by Farnan and Salje (2001), the isolated $Q^0$ species in crystalline zircon was observed at the very end of the range for $Q^0$ species in Al-free crystalline silicates. As a

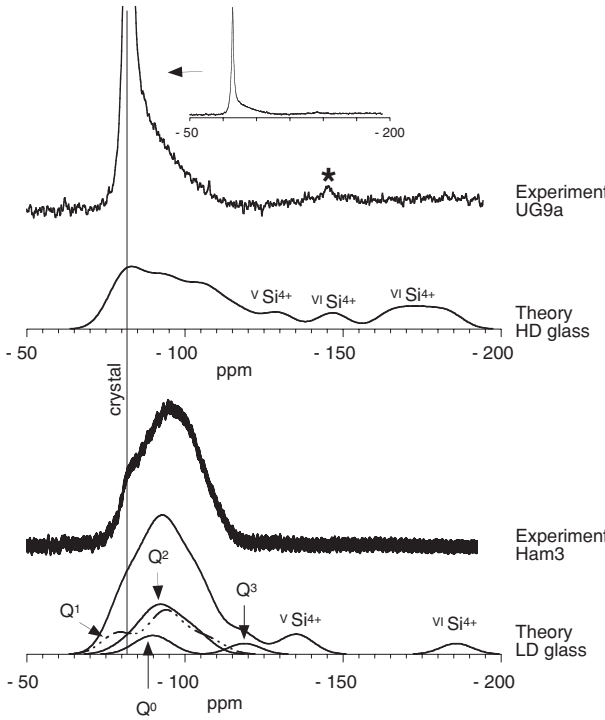


**FIGURE 8.** Theoretical and experimental $^{29}$Si NMR spectra. The UG9a sample has experienced a radiation dose of $1.8 \times 10^{18}$ α-decay/g (Farnan 1999). The Ham3 has experienced a dose higher than that of the percolation transition ($>8 \times 10^{18}$ α-decay/g) (Farnan and Salje 2001). The elevated proportion of highly coordinated Si atoms in the theoretical HD glass does not allow the definition of true $Q^n$ species. Star: spinning side band.

consequence the NMR $Q^n$ scale in zircon could be somewhat different from that observed in alkali silicate glasses.

The analysis of the $Q^n$ species was only performed on the LD zircon glass. Indeed, the high proportion of five and sixfold coordinated Si atoms in the HD glass does not allow the definition of true $Q^n$ linkages, which should only involve fourfold coordinated Si atoms (Table 1). Despite the poor statistics related to the small number of Si atoms used in the simulations, our calculations on the LD glass confirm that the NMR spectra of amorphous zircon cannot simply be interpreted by considering a regular scale of $Q^n$ species extending between crystalline zircon ($Q^0$) and quartz or amorphous silica ($Q^4$). Indeed, one of the $Q^1$ species shows a chemical shift higher (less negative) than that observed for the $Q^0$ species in the crystalline and in the amorphous phases. Note that the tail of the signal ascribed to the amorphous phase in the experimental spectra extends up to chemical shift values slightly less negative than those measured for crystalline zircon. Furthermore, the $Q^1$ and $Q^2$ species cover a similar broad range of chemical shifts and cannot be unambiguously distinguished using their NMR signal. Finally, the $Q^3$ species appeared at a chemical shift (–119 ppm) more negative than that expected for the $Q^4$ species from the analysis of $SiO_2$ glass (between –100 and –120 ppm; Kirkpatrick 1988). Our theoretical results suggest that the experimental spectra most likely correspond to $Q^0$, $Q^1$, and $Q^2$ species with a much smaller amount of $Q^3$ and $Q^4$ species. The overlapping ranges of chemical shifts for the various $Q$ species makes it difficult to determine the average polymerization in metamict zircon. However, the average polymerization observed in the LD glass ($Q^{1.5}$) leads to a very good agreement between theory and experiment (sample Ham3, Fig. 8). The average polymerization of Si species in natural metamict zircon could thus be similar to that observed in the LD glass.

Fivefold and sixfold coordinated Si species show chemical shifts close to –130 ppm and between –145 and –200 ppm, respectively. In classical molecular dynamics, the observation of highly coordinated Si is often related to some weakness in the parameterized potentials. In the present study, the use of an ab initio code, together with their observation in both the liquid and solid glassy states, strongly suggests that these species are not artifacts related to the description of inter-atomic interactions. However, they were not observed in the experimental spectra of metamict zircon.

## DISCUSSION

The evolution of pressure during the molecular dynamics simulations led to several observations. The pressure calculated for the amorphous phase produced at the crystal volume (HD glass) is close to zero. The HD glass is thus not expected to apply any significant stress over surrounding regions of the same density (Fig. 1). Provided that the properties of the HD glass are similar to those of the amorphous phase observed in weakly damaged zircons, in which the density of the glass is imposed by the embedding crystalline regions, our results suggest that the permanent strain observed in the crystalline part of these samples (Salje et al. 1999) was not directly induced by the presence of the amorphous phase. We can also point out the fact that the equilibrium volume of our high-temperature LD liquid state was close to that of fully metamict zircons, whereas a significant pressure existed in the HD liquid state obtained at the crystal volume. According to classical molecular dynamics modeling of cascade formation, the significant macroscopic swelling of metamict zircon (+18%) would arise from the overlap of damaged regions and not from the structure of the amorphous domains themselves (Trachenko et al. 2002). Following this hypothesis, our results suggest that the density of the amorphous phase assymptotically reached during the amorphization of zircon could be that of the high temperature liquid state, i.e., the density for which the cascade formation does not exert any more transitory stress over the surrounding medium.

The "solid state" expansion of the HD glass to the LD molar volume, performed by simulated annealing, led only to relatively small structural changes. In particular, the recovery of the fourfold coordination observed in the LD glass occurred only via the liquid state. By implication, the increase of the degree of polymerization observed in metamict zircon as a function of the radiation dose (Farnan and Salje 2001) was probably not simply due to a relaxation brought on by the macroscopic swelling. It is more likely that repeated recoil events occurring in the presence of less stringent volume constraints caused the more polymerized amorphous phase to form.

The average polymerization of Si species assessed in

metamict zircon has important consequences on the scale of heterogeneity of the amorphous phase. The general question of glass formation in orthosilicate composition relies on the fact that polymerization (formation of Si-O-Si) must be accompanied by the formation of "free oxide," i.e., the formation of Zr-O-Zr bonds where no Si is involved. Farnan and Salje (2001) pointed out that given the existing empirical correlation between chemical shifts and silicate glass structure, the broad line with a center of gravity at –96 ppm would correspond to $Q^3$ average polymerization. Such a high degree of polymerization would leave 1.5 O atoms unaccounted for per $SiO_4$ tetrahedron in the amorphous phase and would require a significant segregation of Zr oxide. In contrast, our results show that an average polymerization of $Q^{1.5}$ could account for the NMR spectra of metamict zircon. This lower average polymerization is consistent with a non-uniform model for the structure of metamict zircon in which the clustering of cations would be limited to a few coordination polyhedra (Ellsworth et al. 1994). In the high temperature liquid, the polymerization of Si species, which is related to the production of "free" O atoms and the breaking of Zr-O-Si bonds, could lead to the unmixing of crystalline $ZrO_2$ (Butterman and Foster 1967).

The dielectric properties suggest a greater structural disorder in the theoretical LD glass compared to metamict zircon. Significant discrepancies are also observed in the first coordination shell of the cations: five and sixfold coordinated Si species and a broader distribution of Zr-O distances were observed in the theoretical glasses. These highly coordinated Si species and distorted Zr polyhedra appear as important transition states in the liquid dynamics. Three interpretations can be made given their absence in the natural samples of metamict zircon. First, the five and sixfold coordinated Si atoms are mainly observed in the HD glass phase. Thus, they should occur preferentially in the weakly damaged samples with a low amorphous fraction constrained by the surrounding crystalline phase. However, careful NMR experiments with long-time recording did not reveal the presence of highly coordinated species in the moderately damaged zircon samples. Second, the very rapid quench of the liquid may lead to the preservation of highly unstable species in the solid state whereas radiation damage could produce a different amorphous structure. However, the quench rate in our calculation was similar to that inferred from classical molecular dynamics investigations (Crocombette and Ghaleb 2001; Trachenko et al. 2002). The observation of highly coordinated species in these studies, both in the cascades of defects and in the glasses produced by quenching the melt, suggests that these species are not specific of quenched zircon melts but can be produced by radiation damage. In a more likely interpretation, their annealing could have occurred on a time scale exceeding the possibility of molecular modeling. In particular, we can note that most of the experimental investigations were performed on naturally amorphized samples, which were submitted to long term annealing processes. These processes have likely resulted in local re-organization of the amorphous structure leading to the complete recovery of fourfold coordinated Si species and regularization of Zr coordination polyhedra. The presence of minor amounts of hydroxyls in the structure of natural zircons (Woodhead et al. 1991; Nasdala et al. 2001) may have also contributed to the annealing of the high energy molecular configurations and to the subsequent relaxation of the structure of the zircon glass. Note that the transformation from five and six to fourfold coordinated Si species in the HD glass is likely to generate a significant stress over the surrounding medium and could be an alternative explanation for the swelling of metamict zircons. Further experiments on artificially amorphized synthetic zircon together with the determination of the annealing pathways of the high-energy species should shed light on this question.

## ACKNOWLEDGMENTS

We thank T. Geisler-Wierwille and two anonymous referees for their constructive comments. The work of CJP was supported by EPSRC in the U.K. and Université of Paris 7 in France. Calculations were performed at the IDRIS institute (Institut du Développement et des Ressources en Informatique Scientifique) of CNRS (Centre National de la Recherche Scientifique). This work was supported by the IPGP-Cambridge collaboration. This is IPGP contribution number 1896.

## REFERENCES CITED

Ankudinov, A.L., Ravel, B., Rehr, J.J., and Conradson, S.D. (1998) Real space multiple scattering calculation and interpretation of X-ray absorption near edge structure. Physical Review B, 58, 7565.

Balan, E., Neuville, D.R., Trocellier, P., Fritsch, E., Muller, J.-P., and Calas, G. (2001a) Metamictization and chemical durability of detrital zircon. American Mineralogist, 86, 1025–1033.

Balan, E., Mauri, F., Muller, J.-P., and Calas, G. (2001b) First principles study of water adsorption on the (100) surface of zircon: Implications for zircon dissolution. American Mineralogist, 86, 910–914.

Balan, E., Saitta, A.M., Mauri, F., and Calas, G. (2001c) First-principles modeling of the infra-red spectrum of kaolinite. American Mineralogist, 86, 1321–1330.

Baroni, S., de Gironcoli, S., Dal Corso, A., and Giannozzi, P. (2001) Phonons and related crystal properties from density-functional perturbation theory. Reviews of Modern Physics, 73, 515–561.

Brese, N.E. and O'Keefe, M. (1991) Bond-Valence Parameters for Solids. Acta Crystallographica B, 47, 192–197.

Butterman, W.C. and Foster, W.R. (1967) Zircon stability and the $ZrO_2$-$SiO_2$ phase diagram. American Mineralogist, 52, 880–885.

Calas, G. and Petiau, J. (1993) Structure of oxide glasses. Spectroscopic studies of local order and crystallochemistry. Geochemical implications. Bulletin de Minéralogie, 106, 33–55.

Car, R. and Parrinello, M. (1985) Unified approach for molecular dynamics and density-functional theory. Physical Review Letters, 55, 2471–2474.

Crocombette, J.-P. and Ghaleb, D. (1998) Modeling the structure of zircon ($ZrSiO_4$): empirical potentials, ab initio electronic structure. Journal of Nuclear Materials, 3, 282–286.

——— (2001) Molecular dynamics modeling of irradiation damage in pure and uranium-doped zircon. Journal of Nuclear Materials, 295, 167–178.

Devanathan, R., Weber, W.J., and Corrales, L.R. (2002) Atomistic Simulation of Displacement Cascades in Zircon. In B.P. McGrail and G.A. Cragnolino, Ed., Scientific Basis for Nuclear Waste Management XXV, 713, 1–8. Materials Research Society, Warrendale, PA.

Ellsworth, S., Navrotsky, A., and Ewing, R.C. (1994) Energetics of Radiation Damage in Natural Zircon ($ZrSiO_4$). Physics and Chemistry of Minerals, 21, 140–149.

Ewing, R.C. (1999) Nuclear waste forms for actinides. Proceedings of the National Academy of Sciences, 96, 3432–3439.

Ewing, R.C., Haaker, R.F., and Lutze, W. (1982) Leachability of zircon as a function of alpha dose. Scientific Basis for Radioactive Waste Management, 5, 389–397.

Farges, F. and Calas, G. (1991) Structural analysis of alpha-irradiation damage in zircon and thorite: a X-ray absorption study. American Mineralogist, 76, 60–73.

Farnan, I. (1999) $^{29}$Si NMR characterisation of the crystalline-amorphous transition in $ZrSiO_4$. Phase Transitions, 69, 47–60.

Farnan, I. and Salje, E.K.H. (2001) The degree and nature of radiation damage in zircon observed by $^{29}$Si nuclear magnetic resonance. Journal of Applied Physics, 89, 2084–2090.

Farnan, I., Balan, E., Pickard, C.J., and Mauri, F. (2003) The effect of radiation damage on local structure in crystalline $ZrSiO_4$: Investigating the $^{29}$Si NMR response to pressure in zircon and reidite. American Mineralogist, 88, 1663–1667.

Frenkel, D. and Smit, B. (1996) Understanding molecular simulation. From algorithms to applications, 444 p. Academic Press Limited, San Diego.

Galoisy, L., Pélegrin, E., Arrio, M.A., Ildefonse, P., Calas, G., Fillet, C., and Pacaud, F. (1999) Evidence for 6-coordinated Zr in inactive nuclear waste glasses. Journal of the American Ceramics Society, 82, 2219–2224.

Geisler, T., Pidgeon, R.T., van Bronswijk, W., and Kurtz, R. (2002) Transport of

uranium, thorium, and lead in metamict zircon under low-temperature hydrothermal conditions. Chemical Geology, 191, 141–154.
Hazen, R.M. and Finger, L.W. (1979) Crystal structure and compressibility of zircon at high pressure. American Mineralogist, 64, 196–201.
Holland, H.D. and Gottfried, D. (1955) The effect of nuclear radiation on the structure of zircon. Acta Crystallographica, 8, 291–300.
Hutter, J., Ballone, P., Bernasconi, M., Focher, P., Fois, E., Goedecker, St., Parrinello, M., and Tuckerman, M. (1996) CPMD Version 3.0. MPI für Festkörper forschung Stuttgart and IBM Research.
Kirkpatrick, R.J. (1988) MAS NMR spectroscopy of minerals and glasses. In F.C. Hawthorne, Ed., Spectroscopic Methods in Mineralogy and Geology, 18, 341–403. Reviews in Mineralogy, Mineralogical Society of America, Washington, D.C.
Kleinman, L. and Bylander, D.M. (1982) Efficacious form for model pseudopotentials. Physical Review Letter, 48, 1425–1428.
Maekawa, H., Maekawa, K., Kawamura, K., and Yokokawa, T. (1991) The structural groups of alkali silicate glasses determined from $^{29}$Si MAS-NMR. Journal of Non-Crystalline Solids, 127, 53–64.
Meldrum, A., Boatner, L.A., Weber, W.J., and Ewing, R.C. (1998) Radiation effects in zircon and monazite. Geochimica et Cosmochimica Acta, 62, 2509–2520.
Murakami, T., Chakoumakos, B.C., Ewing, R.C., Lumpkin, G.R., and Weber, W.J. (1991) Alpha-decay event damage in zircon. American Mineralogist, 76, 1510–1532.
Nasdala, L., Beran, A., Libowitzky, E., and Wolf, D. (2001) The incorporation of hydroxyl groups and molecular water in natural zircon ($ZrSiO_4$). American Journal of Science, 301, 831–857.
Perdew, J.P., Burke, K., and Ernzerhof, M. (1996) Generalized gradient approximation made simple. Physical Review Letter, 77, 3865–3868.
Pickard, C.J. and Mauri, F. (2001) All-electron magnetic response with pseudopotentials: NMR chemical shifts. Physical Review B, 63, 245101.
Qi, W.-J., Nieh, R., Dharmarajan, E., Lee, B.H., Jeon, Y., Kang, L., Onishi, K., and Lee, J.C. (2000) Ultrathin zirconium silicate film with good thermal stability for alternative gate dielectric application. Applied Physics Letter, 77, 1704–1706.
Rignanese, G.M., Gonze, X., and Pasquarello, A. (2001) First-principles study of structural, dynamical, and dielectric properties of zircon. Physical Review B, 63, 104305.
Rignanese, G.M., Detraux, F., Gonze, X., Bongiorno, A., and Pasquarello, A. (2002) Dielectric constant of Zr silicates: A first-principles study. Physical Review Letters, 89, 117601.
Ríos, S., Salje, E.K.H., Zhang, M., and Ewing, R.C. (2000) Amorphization in zircon: evidence for direct impact damage. Journal of Physics: Condensed Matter, 12, 2401–2412.
Salje, E.K.H., Chrosch, J., and Ewing, R.C. (1999) Is "metamictization" of zircon a phase transition? American Mineralogist, 84, 1107–1116.
Stebbins, J.F. (1995) Nuclear magnetic resonance spectroscopy of silicates and oxides in geochemistry and geophysics. In T.J. Ahrens, Ed., Minerals Physics and Crystallography, A Handbook of Physical Constants, 303–331 p. American Geophysical Union, Washington, D.C.
Trachenko, K.T., Dove, M.T., and Salje, E. (2001) Atomistic modeling of radiation damage in zircon. Journal of Physics: Condensed Matter, 13, 1947–1959.
——— (2002) Structural changes in zircon under α-decay irradiation. Physical Review B, 65, 180102.
Troullier, N. and Martins, J.L. (1991) Efficient pseudopotentials for plane-wave calculations. Physical Review B, 43, 1993–2006.
Wang, S.X., Wang, L.M., and Ewing, R.C. (2000) Irradiation-induced amorphization: Effects of temperature, ion mass, cascade size and dose rate. Physical Review B, 63, 024105.
Weber, W.J., Ewing, R.C., and Wang, L.-M. (1994) The radiation-induced crystalline-to-amorphous transition in zircon. Journal of Materials Research, 9, 688–698.
Wilk, G.D., Wallace, R.M., and Anthony, J.M. (2000) Hafnium and zirconium silicates for advanced gate dielectrics. Journal of Applied Physics, 87, 484–492.
Woodhead, J.A., Rossman, G.R., and Thomas, A.P. (1991) Hydrous species in zircon. American Mineralogist, 76, 1533–1546.
Zhang, M. and Salje, E.K.H. (2001) Infrared spectroscopy analysis of zircon: Radiation damage and the metamict state. Journal of Physics: Condensed Matter, 13, 3057–3071.

MANUSCRIPT RECEIVED OCTOBER 28, 2002
MANUSCRIPT ACCEPTED APRIL 13, 2003
MANUSCRIPT HANDLED BY MICHAEL FECHTELKORD